Green preparation and properties of superhydrophobic stainless steel surfaces

Y. Y. Wu [a], X. Ye [a,*], X. H Yang [b,c], Y. Zhou [a], R. Chao [a], M. X. Kuang [a], Y. H He [a]
a School of Mechanical Engineering, Jiangsu University of Technology, Chang-zhou 213001, China
b School of Materials Engineering, Jiangsu University of Technology, Changzhou 213001, China
c School of Materials Science and Engineering, Changzhou University, Chang-zhou 213164, China

In this paper, a green and efficient method for preparing superhydrophobic stainless steel surface is presented. A periodic grating structure was fabricated on the surface of 304 stainless steel using nanosecond laser pulses, and then chemically modified with myristic acid, an environmentally friendly reagent. This approach successfully achieved durable and robust superhydrophobic properties on stainless steel surfaces with a contact angle of 156.5 ° and a roll angle of 2.8 °. The surface remains excellent hydrophobicity after undergoing various abrasion impact tests. The proposed preparation method is helpful in promoting the industrial application of stainless steel.

1. Introduction

Superhydrophobic surfaces have received considerable focus owing to their unique wettability and a suite of functionalities such as self-cleaning [1-3], droplet transport [4], anti-icing [5], oil-water separation [6], drag reduction [7, 8], and corrosion protection [9], highlighting their substantial potential for engineering applications. Currently, numerous studies have successfully fabricated superhydrophobic surfaces on various materials using methods such as sol-gel [10], template [11, 12], laser etching [13], chemical etching [14], chemical vapor deposition [15], and electrodeposition [16]. Stainless steel, renowned for its excellent corrosion resistance and ease of processing, is extensively utilized in construction, chemical industry, aerospace, and other fields [17, 18]. Through the preparation of a superhydrophobic stainless steel surface, a range of new functionalities is introduced alongside the acquired hydrophobicity, thereby broadening the application scope of stainless steel.

In recent years, numerous researchers have employed diverse methods to fabricate superhydrophobic stainless steel surfaces. Yang et al. [19] employed electric spark deposition and electrochemical etching techniques to fabricate durable structures on the Q235 steel surface. Following the modification treatment, the treated surface showed a contact angle of 159° ± 2° and demonstrated superior wear resistance. Xu et al. [20] proposed a novel approach to the fabrication of superhydrophobic stainless steel mesh via magnetic field-assisted jet electrodeposition, incorporating ferromagnetic nickel particles (Nip) into the plating solution, resulting in a Ni-Nip coating with a mountainous roughness structure on stainless steel meshes. After 6 days of air exposure, the coating spontaneously transitioned from superhydrophilicity to superhydrophobicity and manifested superoleophilicity, thereby achieving effective separation of oil-water mixtures. Wang et al. [21]. successfully developed a ZnS superhydrophobic coating on 316L stainless steel via a combination of electrodeposition, solvothermal synthesis and chemical modification processes, achieving water contact and rolling angles of 160.06° and 3°, respectively. Deng et al. [22] utilized a sol-gel method or electrochemical deposition to prepare a superhydrophobic ZnO seed layer on 304 stainless-steel (304SS).

This structure exhibited significant anti-icing properties. Zhang et al. [23] successfully fabricated a superhydrophobic stainless steel surface achieving a water contact angle of 162.45° and a rolling angle of 4.8° via room temperature HF etching followed by stearic acid modification. Although the aforementioned methods can fabricate superhydrophobic surfaces with excellent performance, they may involve corrosive chemical reagents or complex processes. Laser machining, a high-precision, non-contact method, is frequently utilized to fabricate stable micron structures on metal substrates [24].Srin K S et al.[25] employed femtosecond laser to fabricate periodic nano-microstructures with varying morphologies on untreated AISI 304 stainless steel, resulting in a hydrophobic surface with apparent contact angles ranging from 110° to 135°.Sun et al.[26] fabricated a superhydrophobic 304 stainless steel surface (SHS) with controllable periodic structures using picosecond laser technology, demonstrating a remarkable anti-biological fouling effect. Pan et al. [27] employed picosecond laser technology to fabricate a superhydrophobic and antibacterial surface on AISI 420 martensitic   stainless-steel substrates, capable of resisting 99% of E. coli and 93% of Staphylococcus aureus adhesion, with virtually no bacterial adhesion at rest. Tang et al. [28] introduced a novel technique for fabricating superhydrophobic surfaces using femtosecond laser-chemical methods, creating a superhydrophobic surface on 316L stainless steel to enhance its wear resistance and corrosion resistance. Zhao et al. [29] developed a metallic superhydrophobic surface with anisotropic wettability by combining pulsed laser ablation with low-temperature annealing post-treatment. Given that the aforementioned methods require expensive femtosecond or picosecond pulsed lasers, developing a low-cost and environmentally friendly approach for fabricating superhydrophobic stainless steel surfaces offers significant advantages. Myristic acid, naturally occurring in plant oils as glycerides, is frequently employed in the food industry for the preparation of a broad spectrum of edible flavors. [30]. Compared to silanes with low surface energy, myristic acid offers advantages in terms of safety and economy.

In this study, a grating array with rough structures were prepared on stainless steel surfaces using an eco-friendly and highly efficient nanosecond laser. Subsequently, the stainless-steel surface was rendered superhydrophobic through modification with the eco-friendly agent, myristic acid. The impact of laser processing parameters and modification duration on the surface wettability was investigated. The self-cleaning, stain resistance properties, and stability of the modified surface were evaluated. The test results demonstrate that the surface exhibits superior self-cleaning and anti-fouling properties, maintaining remarkable stability even under a wide range of adverse conditions. This research presents a facile and environmentally sustainable approach to fabricating superhydrophobic surfaces on stainless steel, potentially broadening its applications in complex working environments.

2. Materials and methods

2.1. Materials

Stainless steel plate (304,40 mm×20mm×3mm, Xinghua Qiangsheng Stainless Steel Metal Products Factory), Deionised water (Blue Ocean Water Purification Equipment Co., Ltd.), myristic acid, anhydrous ethanol, hydrochloric acid (HCl) and sodium hydroxide (NaOH) (analytically pure, all purchased from Sinopharm Chemical Reagent Co., Ltd.).

2.2. Sample preparation

The stainless-steel plates were ultrasonically cleaned with anhydrous ethanol for 10 min and subsequently dried (denoted as S0). The sample（S0） was mounted onto an infrared nanosecond laser marking system (DL-TG-IRF-30, DelphiLaser, China) for surface etching under predefined parameters. The etched sample was ultrasonically cleaned in absolute ethanol for 10 minutes to remove loose slag on the surface, then dried for subsequent use (denoted as S1). Both S0 and S1 samples were soaked in a 0.05 mol/L ethanol solution of myristic acid for 1 to 4 hours for surface modification. Following the modification, the samples were removed, ultrasonically cleaned for 5 minutes to eliminate residual myristic acid, and subsequently placed in an oven for drying. The drying process was conducted at 60°C for 40 minutes. The S0 surface modified with myristic acid was labeled as S2. Fig. 1 presents a schematic diagram depicting the sample preparation process. To

determine the optimal process parameters, an orthogonal experiment was designed with laser power (p), step size (d), scanning speed (v), and modification time (t) as variables as the four factors, as depicted in Table 1.
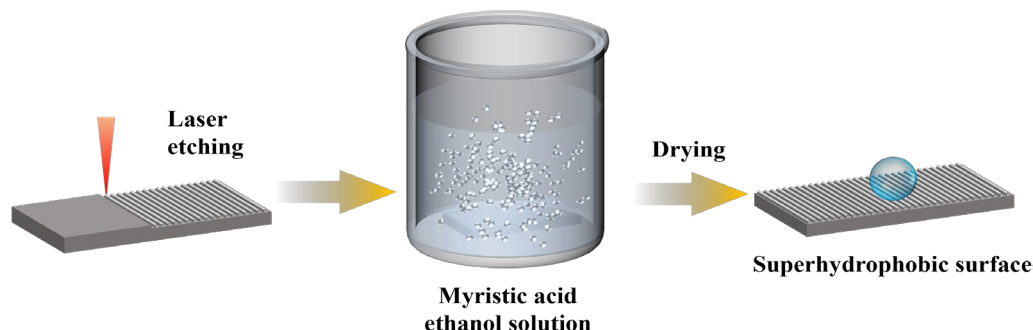

Fig. 1. Schematic diagram of sample preparation.

Table 1. Level-factor of orthogonal experiment.

Level	Factor			
	A	B	C	D
	Power/w	Step size/μm	Speed/mm/s	Modification/h
1	15	100	100	1
2	20	200	200	2
3	25	300	300	3
4	30	400	400	4

2.3. Sample characterization

The water contact angle (WCA) and water sliding angle (WSA) of the sample surface were measured utilizing a contact angle goniometer (DSA-30, Kruss, Germany). During the measurement, 6 μL of distilled water was dispensed at 5 different positions on the sample surface, and the final results were reported as mean values. Scanning electron microscopy (EVOMA 10, Zeiss, Germany) operating at 20 kV was utilized to observe the surface micromorphology of the samples, while energy dispersive spectroscopy (EDS) was utilized to analyze their surface elemental composition. The samples' three-dimensional profiles and roughness were obtained using a laser scanning confocal microscope (VT6000, CHOTEST, China). Fourier Transform Infrared Spectrometer (FTIR Spectrometer) (ALPHA, BRUKER, Germany) was utilized to identify the functional groups present on the sample surfaces.

2.4. Stability testing

The samples were fixed on a friction wear testing machine to perform cyclic wear tests. Sandpaper (800#) and steel wool were used under a 100 g load to abrade the SHS surface, with each wear cycle covering a distance of 40 mm. Following the wear test, the WCA and WSA of the samples were determined to assess their wear resistance. During the adhesive tape peeling test, the sample surface was covered with high viscosity 3M tape., rolled with a 2 kg iron bar, and subsequently peeled off, with each process considered as one cycle in the experiment. In the sand-drop impact test, sand particles were released from an elevation of 30 cm above the sample surface and impacted it. Outdoor degradation tests involved exposing the superhydrophobic samples to ambient environmental conditions. For the chemical etching test, SHS samples were individually submerged in acidic and alkaline solutions with pH levels ranging from 1 to 11 for a duration of 6 hours, after which the WCA and WSA of the surfaces were measured. For the thermal stability test, the prepared samples were placed in a continuously heated oven and a continuously heated water bath,

respectively, at temperatures between 60 °C-160 °C and 20 °C-100 °C, respectively, for 12 hours. at each temperature setting, and then the corresponding surface wettability was measured.

3. Results and discussion

3.1. Effect of process parameters on surface wettability

As shown in Fig. 2 (a-b), the contact angle of the untreated stainless-steel surface (S0) is 47°, indicating hydrophilicity. After treatment with myristic acid (S2), the WCA increased to 95°, demonstrating that low surface energy materials can enhance the hydrophobicity of the surface. According to research, achieving superhydrophobicity typically requires sufficient surface roughness and low surface energy [31].

As shown in Table 2, the orthogonal experimental results indicate that all processing parameters significantly affect the surface wettability of the samples. Based on the range R analysis presented in Table 3, the factors' influence on the surface WCA and WSA follows the order B>D>A>C and A>B>D>C, respectively. Specifically, scanning spacing (B) has the greatest impact on the contact angle, while power (A) most significantly affects the sliding angle. Combined with the K value, it is observed that the processing spacing (B) results in superhydrophobic properties for both 100 μm (B1) and 200 μm (B2). Power (A) of 25W (A3) and 30W (A4) respectively resulted in the maximum WCA and the minimum WSA. The speed (C) has little influence on both, thus a speed of 400mm/s (C4) is selected. The modification time (D) significantly affected both the WCA and WSA, and meets the superhydrophobic requirement under the condition of 4h (D4). On this basis, a validation experiment was conducted to further optimize the synergistic impacts of the two combined factors, and the experimental combination is shown in Table 4. As shown in Fig. 2 (e), all the samples prepared in the validation experiments exhibited superhydrophobic properties. However, under the combination A3B1C4D4 (power: 25W, scanning spacing: 100 μm, scanning speed: 400 mm/s, and modification time: 4 hours), the sample surface achieved the maximum WCA and the minimum WSA. Ultimately, this parameter combination was selected for etching and modifying the stainless-steel surface, with the sample labeled as SHS. After laser etching and modification with myristic acid, the SHS surface exhibited superhydrophobicity, with a WCA and WSA of 156.3 ° and 2.8 °, respectively (Fig. 2 (c-d)).

Table 2. Orthogonal design and experimental results.

Test number	Factor				Results	
	A	B	C	D	WCA/°	WSA/°
	Power/w	Step size/μm	Speed/mm/s	Modification/h		
1	1	1	1	1	149	>20
2	1	2	2	2	148.5	>20
3	1	3	3	3	146.2	16
4	1	4	4	4	150.1	>20
5	2	1	2	3	152.1	12.8
6	2	2	1	4	153	5
7	2	3	4	1	150.1	14.2
8	2	4	3	2	144.1	17.8
9	3	1	3	4	150.9	4.5
10	3	2	4	3	152.3	9.8
11	3	3	1	2	149.8	15.7
12	3	4	2	1	147.5	17.2
13	4	1	4	2	148.4	5.7
14	4	2	3	1	149.8	8.2
15	4	3	2	4	150.7	6.8
16	4	4	1	3	142.9	17

Table. 3 Range analysis of data.

		A	B	C	D
		Power/w	Step size/μm	Speed/mm/s	Modification/h
WCA(°)	k1	148.450	150.100	148.675	149.100
	k2	149.825	150.900	149.700	147.700
	k3	150.125	149.200	147.750	148.375
	k4	147.950	146.150	150.225	151.175
	range R	2.175	4.750	2.475	3.475
WSA(°)	k1	19.000	10.750	14.425	14.900
	k2	12.450	10.750	14.200	14.800
	k3	11.800	13.175	11.625	13.900
	k4	9.425	18.000	12.425	9.075
	range R	9.575	7.250	2.800	5.825

Table 4. Optimal combination verification experimental design.

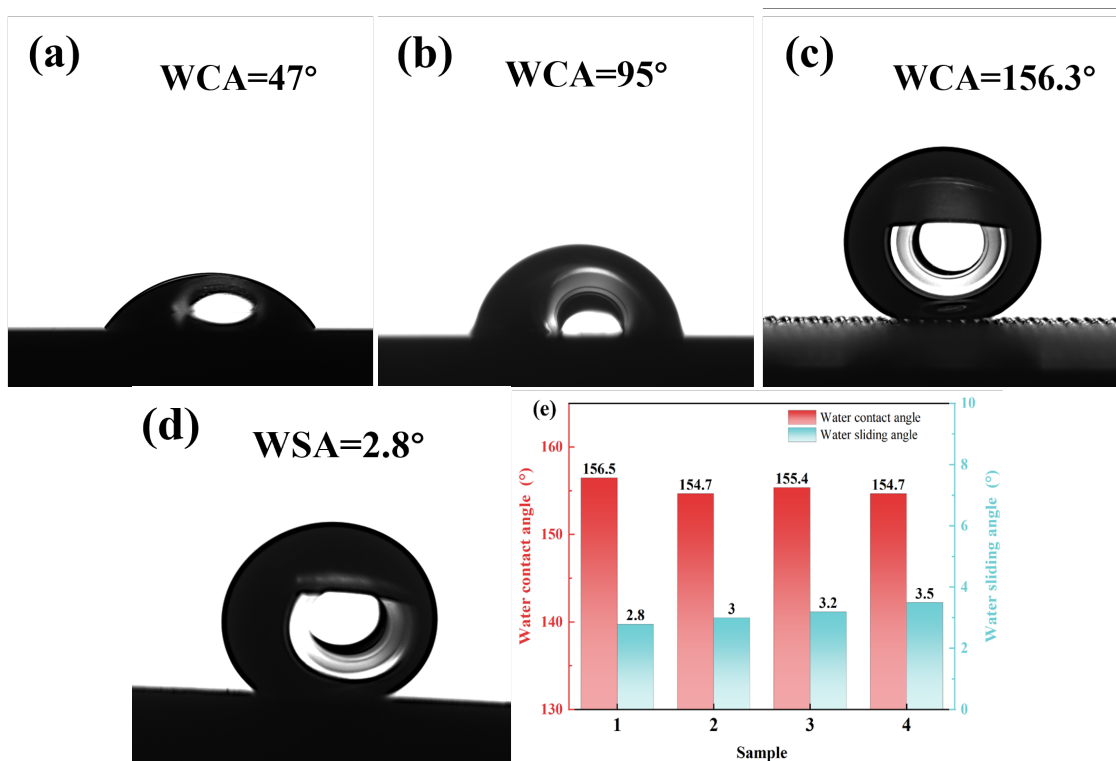| Sample	Power p/w	Step size /μm	Speed /mm/s	Modification /h
1(A3B1C4D4)	25	100	400	4
2(A3B2C4D4)	25	200	400	4
3(A4B1C4D4)	30	100	300	4
4(A4B2C4D4)	30	200	300	4

Fig. 2. (a) WCA of S0 surface, (b) WCA of S2 surface, (c) WCA of SHS surface. (d) WSA of SHS surface. (e) WCA and WSA of confirmatory experimental samples.

3.2. Surface morphology

As illustrated in Fig. 3 (a), repeated laser processing at the same location results in the formation of pits and protrusions on the stainless-steel surface due to the high energy input. Furthermore, molten material and spatter can adhere to adjacent non-processed surfaces, leading to an

increase in protrusion height and the complexity of the microstructure in these regions. It can be seen from the three-dimensional structure diagram taken by confocal photography (Fig. 3 (b)) that the continuous accumulation of slag debris resulted in the formation of complex structures, and the sample's roughness has reached 54.87 μm. As illustrated in Fig. 3 (c-d), post-modification with myristic acid, the SHS samples exhibit a periodic grating array and a sparse distribution of regular microspherical structures on the surface. Additionally, nanoscale "cauliflower"-like cluster structures proliferate on the surfaces of the spherical particles, these nanostructures are crystalline forms of myristic acid.
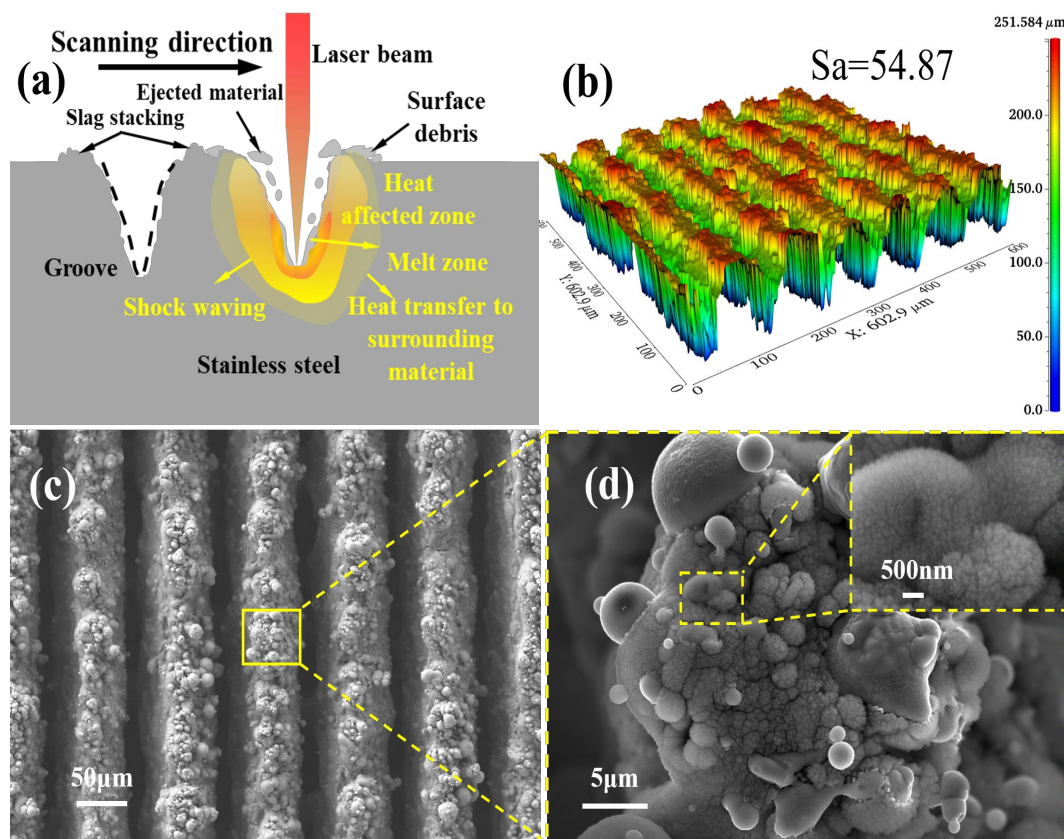
Fig. 3. (a) Schematic diagram of the microstructure produced by laser machining, (b) three-dimensional profile diagram of the S1 surface; (c-d) SEM images of the SHS surface at different magnifications.

3.3. Chemical composition analysis

Surface roughness is a crucial factor influencing the superhydrophobic state, but it does not entirely dictate the wetting behavior. Fig. 4 displays the FTIR spectra of the SHS samples and myristic acid, the infrared spectrum of the SHS sample exhibits stretching vibration peaks for methyl (-CH$_3$) and methylene (-CH$_2$) groups at wavenumbers 2952 cm^{-1}, 2914 cm^{-1}, and 2848 cm^{-1}. A vibration peak for carboxyl groups (-COO-) is observed at a wavenumber of 1694 cm^{-1}. The bending vibration of methylene (-CH$_2$) groups is found in the region around 1463 cm^{-1}. These peaks correspond to the characteristic peaks of myristic acid [32]. The successful attachment of myristic acid to the stainless-steel surface was confirmed through FTIR characterization and analysis.
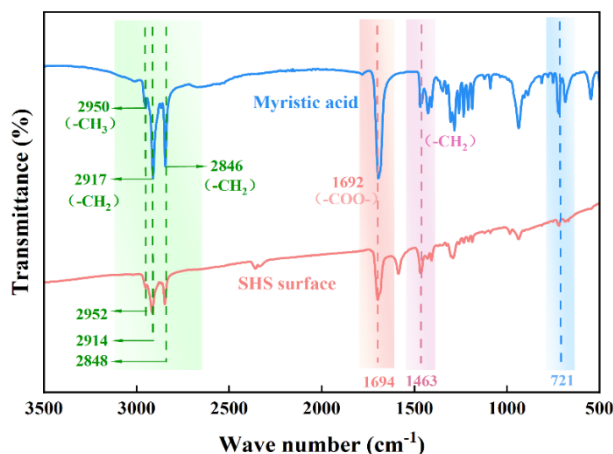
Fig. 4. FTIR spectra of SHS surface and myristic acid.

3.4. Self-cleaning and stain resistance

To assess the self-cleaning and anti-fouling capabilities of SHS, as shown in Fig. 5 (a-b), chalk dust and mud were employed to mimic solid and liquid contaminants respectively, and sprinkled on the S0 surface and SHS surface with an inclination of about 8 °. Drip 3ml water droplets and contaminant liquid on the upper end of the sample through the dropper to observe the residual pollutants. In Fig. 5 (c), due to strong wettability and powder obstruction on the surface of S0, droplets stay and take away part of the powder and slide down after accumulation, but more powder still remains. On the surface of SHS, water droplets tumble down from the upper end and take away the powder on the path (Fig. 5 (d)), showing excellent self-cleaning performance.

As depicted in Fig. 5(e), the slurry spreads over the S0 surface and forms a firmly adhering mud film. On the contrary, the slurry could not stay on the SHS surface and rolled down rapidly without residual slurry adhering to the surface (Fig. 5 (f)). This anti-fouling performance originates from the "air cushion" effect in the rough microstructures of the SHS surface, which makes the mud droplets in a semi-suspended state [31], which reduces the surface adhesion and movement resistance of the mud droplets, allowing them to effortlessly slide off the surface under the influence of gravity, showing excellent anti-fouling performance.
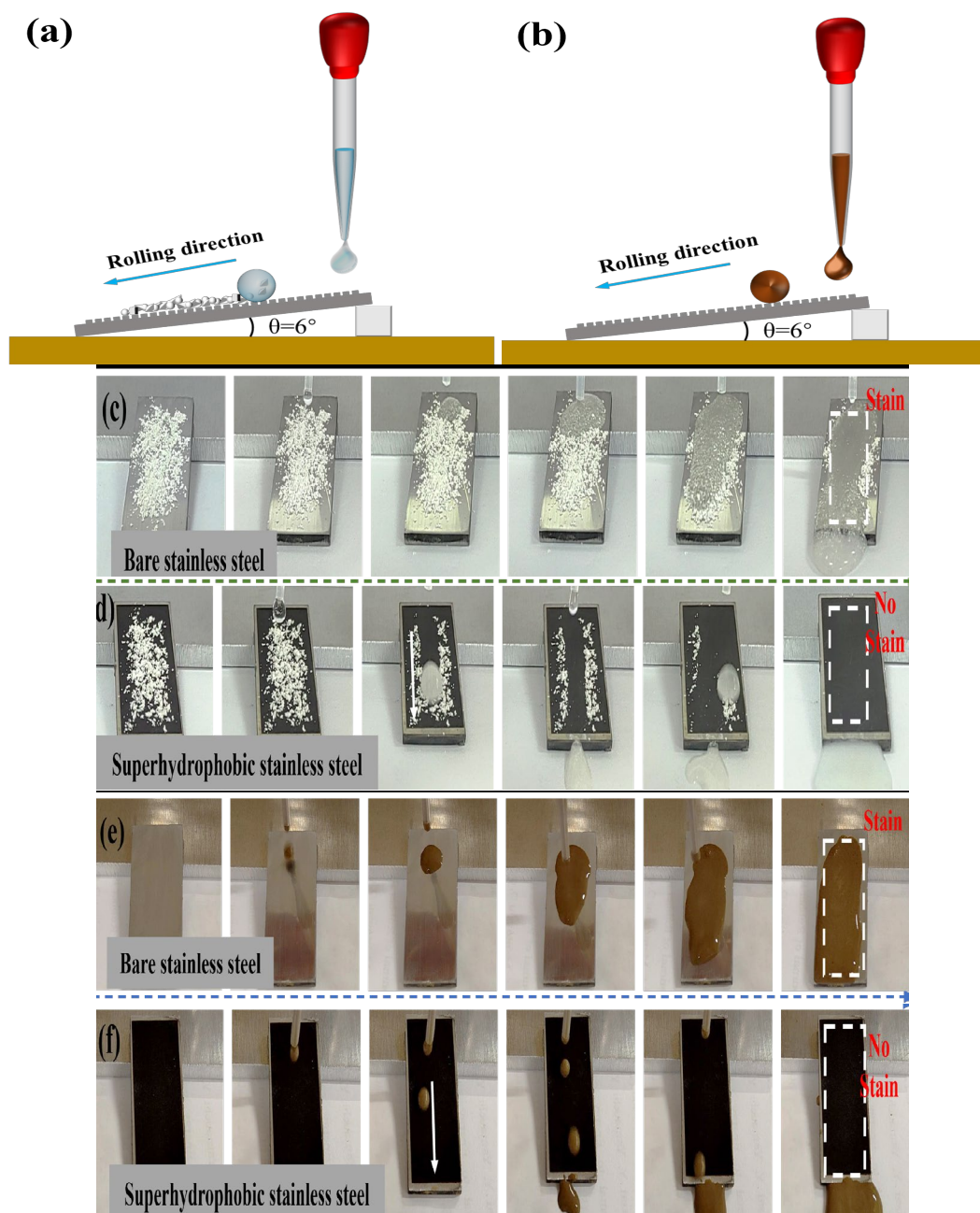
Fig. 5. (a) Schematic diagram of sample surface self-cleaning and (b) anti-fouling test, (c-d) self-cleaning test process, (e-f) anti-fouling test process.

3.5. Abrasion resistance test

Superhydrophobic surfaces with strong mechanical durability are of great significance in practical applications, and sandpaper/steel wool friction and wear are used to evaluate the mechanical durability of samples. The outcomes of the tests are illustrated in Fig. 6 (c-d), after 180 sandpaper frictions (about 12m wear distance), the sample is still superhydrophobic, and the contact angle is 153.2 °; With continued wear to 240 times, the contact angle dropped to 149.6 °. Fig. 6 (e-f) shows the SEM images depicting the surface morphology following 240 cycles of sandpaper abrasion. The microstructures are largely maintained, but the surface nanostructures are damaged by abrasion and the surface is scratched, so the WCA decreases and the WSA rises. Fig. 6 (g-h) depict that after the steel wool was worn 125 times, the surface convex structure was seriously damaged, a large number of "cauliflower" clusters disappeared, the WCA dropped to 148.2 °, and the WSA rose to 26 °, but the surface was still hydrophobic.
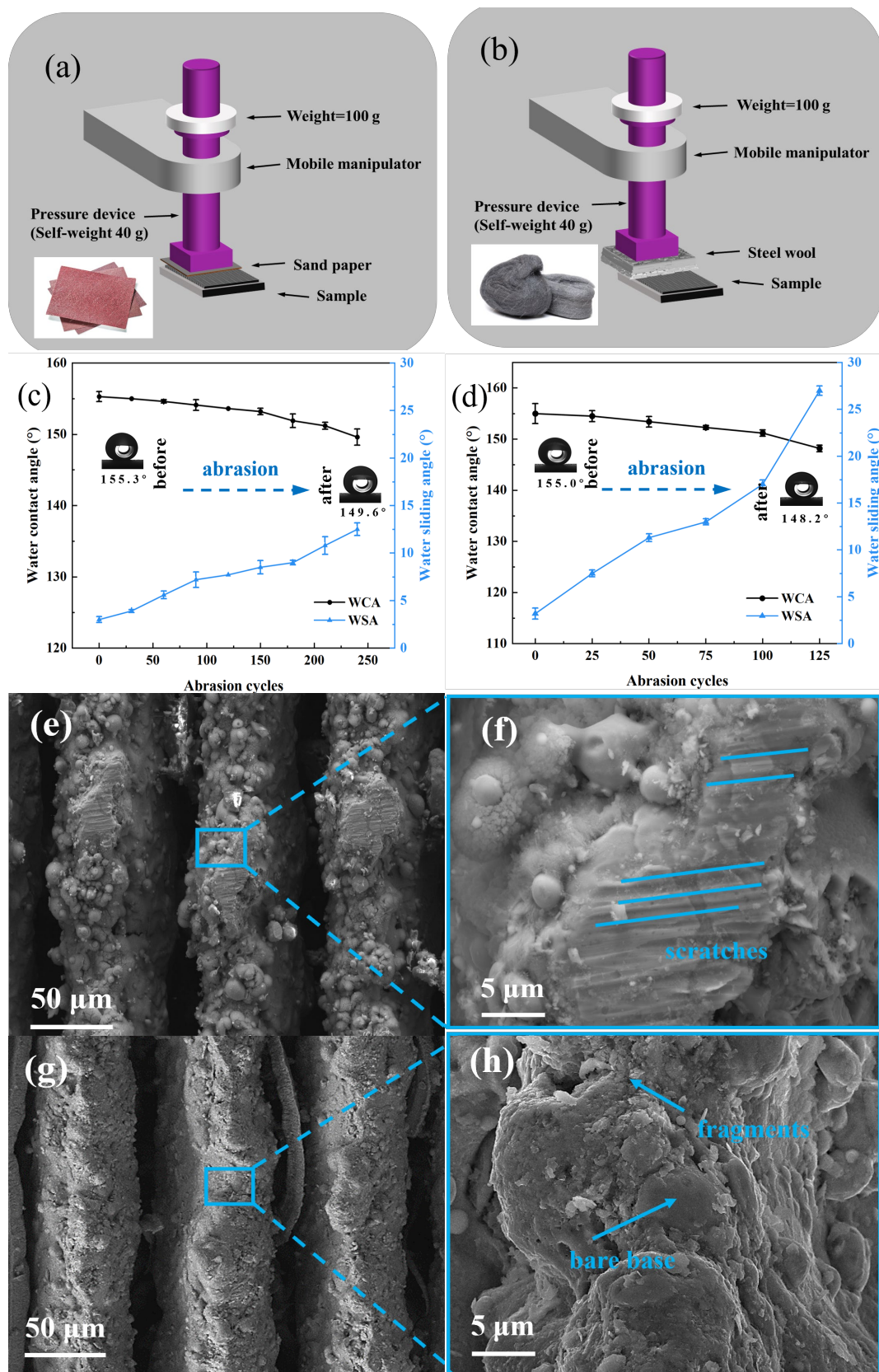
Fig. 6. (a-b) schematic diagrams of the sandpaper/steel wool friction tests, (c-d) depict the changes in WCA and WSA of the SHS samples after the sandpaper/steel wool friction tests, (e-f) show SEM images of the surface after sandpaper abrasion, and (g-h) present SEM images of the surface after steel wool abrasion.

3.6. Other stability tests

To assess the stability of the SHS surface, a series of rigorous conditions were applied, followed by characterization of its wettability post-testing. During the tape peeling test, after 30 peeling cycles, the WCA reduced to 148.1°, while the WSA escalated to 33.1° (Fig. 7(a)), indicating a certain degree of mechanical stability against tape peeling on the SHS surface. The changes in the wettability of the sample under sand impact conditions were further investigated (Fig. 7(b)). When the sand mass reached 90 g, the WSA increased to 9.8°. Even after the sand mass reached 210 g, the WCA remained above 150°, and the WSA rose to 19.7°. As depicted in Fig. 7(c), after prolonged outdoor exposure (21 days), the WCA of the sample remained above 145°, demonstrating excellent stability. In the chemical damage test, SHS samples were separately exposed to acidic and alkaline solutions for 6 hours. For these corrosive solutions, the WCA maintained around 150°, indicating that samples possess excellent chemical durability (Fig. 7(d)). This can be credited to the air cushions trapped by the micro/nano-structures on the SHS surface, which prevent direct contact between the sample and the corrosive solution. Additionally, at various temperatures (60°C - 160°C) or in continuously heated water (20°C - 100°C), the WCA remained above 140°, indicating satisfactory hydrophobicity and suggesting good heat resistance of the SHS surface in both air and water (Fig. 7(e, f)). The above experimental results clearly confirm that the SHS surface maintains excellent stability even under harsh conditions.
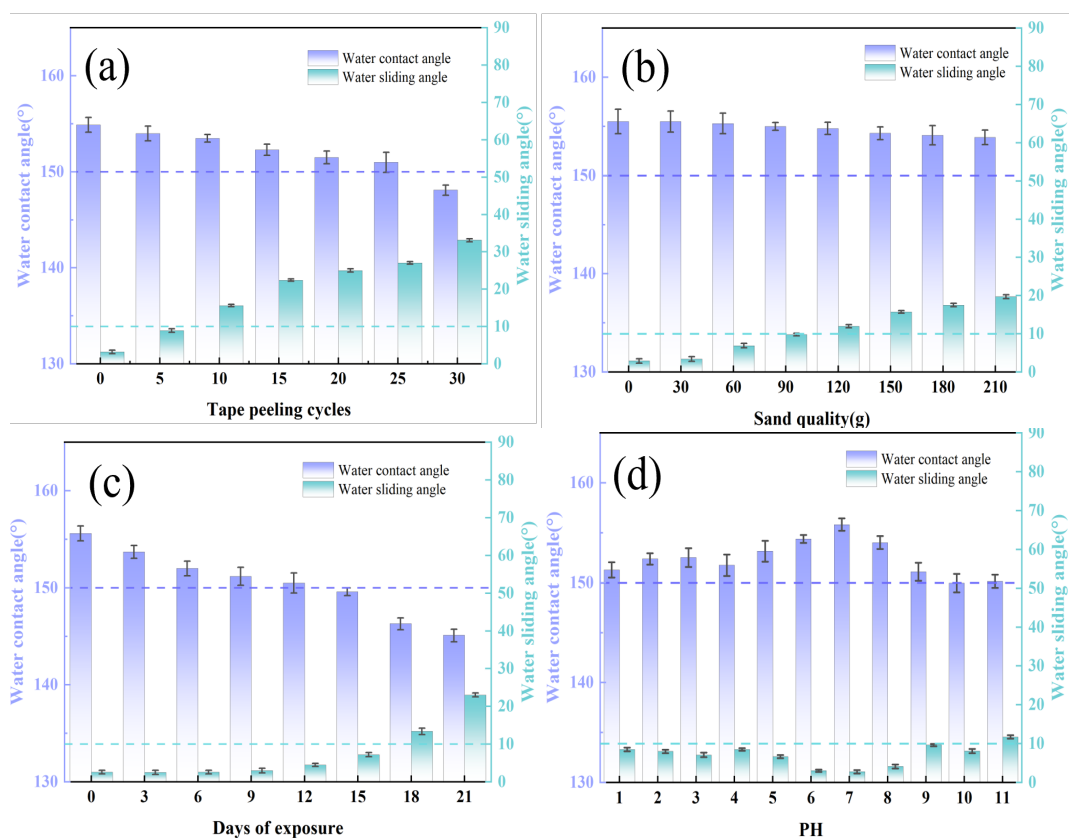

Fig. 7.1. (a-d) the corresponding changes in WCA and WSA for the tape peeling, sand impact, outdoor exposure, acid-base treatment, temperature treatment, and hot water treatment tests, respectively.
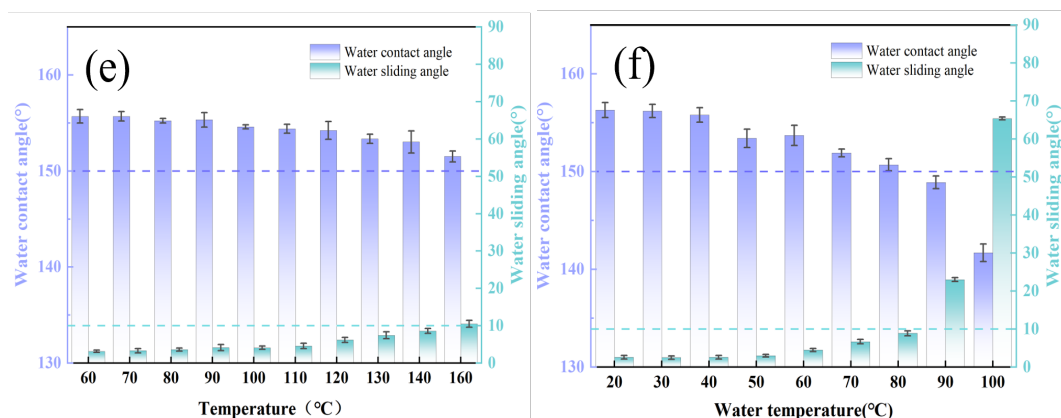
Fig. 7.2. (e-f) the corresponding changes in WCA and WSA for the tape peeling, sand impact, outdoor exposure, acid-base treatment, temperature treatment, and hot water treatment tests, respectively.

4. Conclusion

To realize the green and efficient preparation of superhydrophobic surface on 304 stainless-steel, this paper proposes a method that employs nanosecond laser processing combined with the eco-friendly modifier myristic acid for surface modification. A systematic analysis of the impact of processing parameters on surface wettability was conducted. The results indicated that at a power of 25W, a step size of 100μm, a scanning speed of 400 mm/s, and a modification duration of 4 hours, the resulting surface displayed a WCA of 156.5° and a WSA of 2.8°. Experimental results demonstrated that rolling droplets could effortlessly remove surface contaminants, and sludge showed no adhesion, confirming the surface's exceptional self-cleaning and anti-fouling performance.

During the wear and stability assessments, the surface demonstrated the ability to withstand at least 240 cycles of sandpaper abrasion, 125 cycles of steel wool abrasion, 30 cycles of tape peeling, and a 210g falling sand impact. After being exposed to outdoor conditions for 21 days, the sample retained its hydrophobic properties. After heat treatment between 100°C and 160°C for 24 hours, the WCA of SHS surface remained over 150°. Even after immersion in boiling water for 12 hours, the surface preserved its hydrophobicity, signifying that the SHS possesses excellent thermal stability. In conclusion, the stainless steel superhydrophobic surface fabricated through this method demonstrates remarkable self-cleaning and anti-fouling properties, alongside outstanding stability, offering an effective and environmentally friendly approach for the preparation of superhydrophobic metal surfaces.

Disclosure statement

No potential conflict of interest was reported by the author(s).

Acknowledgements

1892

References

[1] A.K. Deepika, K. Kiranpreet, S. Vickramjeet, Journal of Molecular Liquids 380, (2023); https://doi.org/10.1016/j.molliq.2023.121736

[2] S. F., C. K., A. J., Digest Journal of Nanomaterials and Biostructures 13(3), 693-700(2018);

[3] Y. Zhang, F. Ren, Y. Liu, Applied Surface Science, (2018); https://doi.org/10.1016/j.apsusc.2017.12.019

[4] Q. Sun, D. Wang, Y. Li, J. Zhang, S. Ye, J. Cui, L. Chen, Z. Wang, B. Hans-Jürgen, V. Doris, X. Deng, Nature materials 18(9), 936-941(2019); https://doi.org/10.1038/s41563-019-0440-2

[5] R. Zhang, Z. Ding, K. Wang, H. Zhang, J. Li, Small Methods, (2024); https://doi.org/10.1002/smtd.202301262

[6] Z. Zhang, C. Xu, W. Liu, K. Wang, Y. Rao, C. Jiang, D. Li, Y. Zhang, X. Jiang, X. Chen, C. Xu, Ultrasonics Sonochemistry 81, 105848(2021); https://doi.org/10.1016/j.ultsonch.2021.105848

[7] M. Liravi, H. Pakzad, A. Moosavi, A. Nouri-Borujerdi, Progress in Organic Coatings 140, 105537-105537(2020); https://doi.org/10.1016/j.porgcoat.2019.105537

[8] M. Xu, G. Andrew, N. Yu, K. Gintare, L.J. Won, P.B. R., K.C.J. "Cj", Physical Review Applied 13(3), (2020); https://doi.org/10.1103/PhysRevApplied.13.034056

[9] Z. He, Y. Zeng, M. Zhou, Y. Min, X. Shen, Q. Xu, Langmuir (2020); https://doi.org/10.1021/acs.langmuir.0c03222

[10] B. Aziz, B. Aicha, Z. Mohamed, M. Bouchaib, G. Said, Cellulose 30(10), 6719-6740(2023); https://doi.org/10.1007/s10570-023-05276-8

[11] T.T. Fan, C.H. Xue, X.J. Guo, H.D. Wang, M.C. Huang, D.M. Zhang, F.Q. Deng, Journal of Materials Science 57(22), 10425-10443(2022); https://doi.org/10.1007/s10853-022-07292-8

[12] X. Zhang, C. Wei, Y.-J. Hao, Z.-W. Yan, X. Yan, Y. Chen, X.-J. Guo, W.-Z. Lang, Chemical Engineering Science 282, (2023); https://doi.org/10.1016/j.ces.2023.119325

[13] C.-V. Ngo, D.-M. Chun, CIRP Annals - Manufacturing Technology 67(1), 571-574(2018); https://doi.org/10.1016/j.cirp.2018.04.085

[14] S. Sun, L. Zhu, X. Liu, L. Wu, K. Dai, C. Liu, C. Shen, X. Guo, G. Zheng, Z. Guo, ACS Sustainable Chemistry & Engineering 6(8), 9866-9875(2018); https://doi.org/10.1021/acssuschemeng.8b01047

[15] A.M. Mohammed, A.M. Abdulhakim, D. Rasel, H.S.B. Abd, H.N. Awanis, A.M. Khalid, A.H. Mohammed, N. Mikhail, A.Q. F, H.M. Ali, Scientific Reports 8(1), 2778(2018); https://doi.org/10.1038/s41598-018-21051-3

[16] Y. Wang, G. Zhang, Z. He, J. Chen, W. Gao, P. Cao, Surface & Coatings Technology 464, (2023); https://doi.org/10.1016/j.surfcoat.2023.129548

[17] J.-H. Kim, A. Mirzaei, H.W. Kim, S.S. Kim, Applied Surface Science 439, 598-604(2018); https://doi.org/10.1016/j.apsusc.2017.12.211

[18] Y. Sun, J. Liu, P. Ming, D. Zhao, J. Song, Applied Surface Science 571, (2022); https://doi.org/10.1016/j.apsusc.2021.151269

[19] L. Yang, S. Luo, L. Zheng, T. Zhang, Journal of Materials Science 58(47), 17966-17983(2023); https://doi.org/10.1007/s10853-023-09162-3

[20] J. Xu, Y. Chen, L. Shen, J. Zhao, G. Lou, D. Huang, Y. Yang, Colloids and Surfaces A: Physicochemical and Engineering Aspects 649, (2022); https://doi.org/10.1016/j.colsurfa.2022.129434

[21] K. Wang, S. Yu, X. Yin, L. Liu, L. Wang, G. Zhu, J. Wang, Q. Li, X. Yang, Colloids and Surfaces A: Physicochemical and Engineering Aspects 633(P1), (2022); https://doi.org/10.1016/j.colsurfa.2021.127871

[22] Y. Deng, F. Xu, Z. Yin, M. Xue, Y. Chen, P. He, J. Wu, J. Ou, F. Wang, Y. Luo, Z. Hong, Ceramics International 49(15), 25135-25143(2023); https://doi.org/10.1016/j.ceramint.2023.05.044

[23] Z. Zhang, J. Zhao, Y. Lei, Y. Wang, G. Zhou, C. Xu, Y. Rao, K. Wang, Colloids and Surfaces

A: Physicochemical and Engineering Aspects 586, 124287-124287(2020); https://doi.org/10.1016/j.colsurfa.2019.124287

[24] T.-H. Dinh, C.-V. Ngo, D.-M. Chun, Applied Physics A: Materials Science & Processing 126(6), (2020); https://doi.org/10.1007/s00339-020-03653-9

[25] K.S. Srin, G. Padmanabham, R. Bathe, Materials Performance and Characterization 8(6), 20180090(2019); https://doi.org/10.1520/MPC20180090

[26] K. Sun, H. Yang, W. Xue, A. He, D. Zhu, W. Liu, K. Adeyemi, Y. Cao, Applied Surface Science 436, 263-267(2018); https://doi.org/10.1016/j.apsusc.2017.12.012

[27] Q. Pan, Y. Cao, W. Xue, D. Zhu, W. Liu, Langmuir 35(35), 11414-11421(2019); https://doi.org/10.1021/acs.langmuir.9b01333

[28] T. Yiping, C. Yukui, W. Lei, L. Xichun, W. Bing, S. Qinghua, L. Zhanqiang, Optics and Laser Technology 164, (2023); https://doi.org/10.1016/j.optlastec.2023.109474

[29] Z.Y. Zhe, H.M. Hui, Journal of Central South University 29(10), 3261-3269(2022); https://doi.org/10.1007/s11771-022-5145-z

[30] B.G. A, C.I. G, Food and Chemical Toxicology 45(4), 517-529(2007); https://doi.org/10.1016/j.fct.2006.10.009

[31] H. Luo, Y. Li, D. Huan, C. Zhu, J. Wang, D. Zeng, Polymer-Plastics Technology and Materials 60(10), 1106-1121(2021); https://doi.org/10.1080/25740881.2021.1882490

[32] X. Zhang, H. Yin, J. Tang, C. Hu, T. Li, JOM Journal of the Minerals Metals and Materials Society 73(10), 3111-3120(2021); https://doi.org/10.1007/s11837-021-04814-8